SUPPLEMENTARY INFORMATION

A microfluidic apparatus for the study of ice nucleation in supercooled water drops

Claudiu A. Stan,[a] Grégory F. Schneider,[a] Sergey S. Shevkoplyas,[a] Michinao Hashimoto,[a] Mihai Ibanescu,[b] Benjamin J. Wiley,[a] and George M. Whitesides[a]

[a]*Department of Chemistry and Chemical Biology, Harvard University,* Cambridge, MA 01238 USA

[b]*OmniGuide, Inc.,* Cambridge, MA 01239 USA

Abstract. This supplementary information file contains: i) Tabulated data on the designs of microfluidic channels used for ice nucleation experiments, ii) drawings of the PRTD sensor arrays used for this project, iii) a description of the process of fabricating the PRTD sensor arrays, iv) the calibration procedure for the PRTD sensors, v) derivation of the equations used for the calculation of ice nucleation rates, vi) the generalization of these equations for the case in which the temperature of the channel fluctuates, vii) freezing temperature and cooling rate data for ice nucleation experiments on pure water, and seeded with silver iodide; and viii) six movies of freezing drops inside microfluidic channels.

The design of microfluidic channels used for ice nucleation experiments. The critical geometrical parameters of the flow-focusing generators and of the channels are shown in Figure S-1.

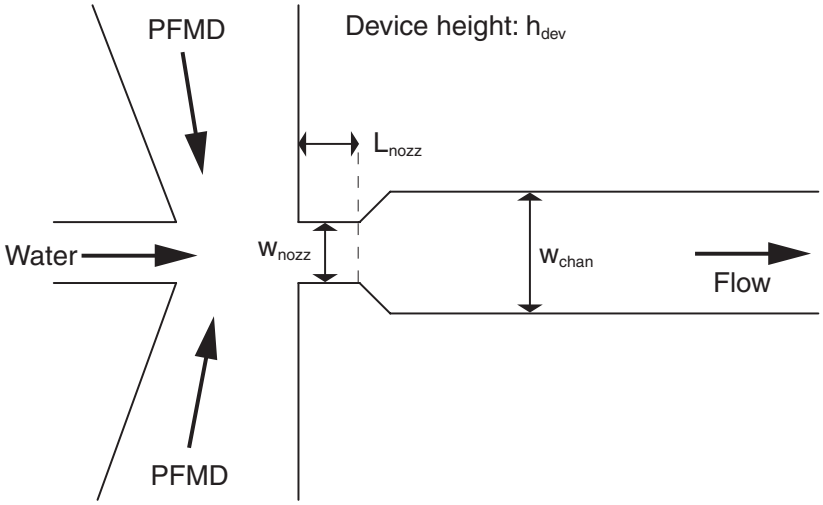

Figure S-1. The critical geometrical design parameters of the microfluidic devices used for the freezing of water drops.

Table ST-1 lists the geometrical parameters for the designs that we used successfully to freeze long trains of water drops. The table also lists the typical operating parameters: the rate of flow of PFMD (Q_{PFMD}), the temperature of the nozzle (T_{nozz}), and the typical diameter (d_{drop}) and frequency (f_{drop}) of the drops during stable operation. During ice nucleation measurements, the drops should be spaced from each other as far as possible to minimize thermal and hydrodynamic interactions between the drops. Since the frequency of generation of drops is proportional to the rate of flow of the water that is fed into the device, it is theoretically possible to reduce the frequency indefinitely, but practically there is a lower frequency limit below which

the generation of the drops becomes disordered. The drop frequency values listed in the table are close to, but above, this lower frequency limit.

The first design listed in Table ST-1 is the one that was used for the measurement of the rate of nucleation of ice. For this design we also list the minimum and the maximum drop diameters that we could achieve by changing the temperature of the nozzle. The second design was used to fabricate the device shown in Figure 6a, and the third design was used to acquire the high-resolution pictures shown in Figure 6b.

Table ST-1. Design parameters for microfluidic devices and typical operating conditions.

#	w_{nozz}(μm)	L_{nozz}(μm)	w_{chan}(μm)	h_{dev}(μm)	Q_{PFMD}(mL/h)	T_{nozz}(ºC)	d_{drop}(μm)	f_{drop}(drop/s)
1	40	70	200	125	3	20	80	50
					3	-2	55	200
					3	35	90	55
2	80	90	300	145	4	20	120	20
3	100	100	400	180	7	20	150	20
4	100	100	400	290	7	20	180	20

Designs for PRTD arrays. Figure S-2 shows drawings of the sensor arrays used for temperature measurement. The design in figure S-2a offered the best optical access to the drops that moved inside the channel, but the lack of symmetry around the midline of the channel made the alignment of the sensor with the channel difficult. The design in Figure S-2b facilitated the alignment of the array to the channel but was used only for the bottom side of the channel since it would mask the drops if placed on top of the channel. The arrays in Figure S-2c and S2-d were symmetric, and had 100-μm and 300-μm wide gaps along their centerlines to allow the optical observation of the drops.

The fabrication of the PRTD arrays. We used 50 mm x 75 mm microscope slides made from soda-lime glass, of from fused silica, as the substrate for the arrays. The slides were cleaned first in a saturated solution of KOH in isopropyl alcohol, then in concentrated H_2SO_4, and finally plasma-etched (Technics Plasma Stripper, model 220; 1 Torr pressure and 100 W RF power) in O_2 for 10 minutes. We spun-coated the slides at 3750 RPM for 20 s, first with a hexamethyldisilazane (HMDS) primer, and then with Microposit S1813 resist; the thickness of the resist layer was ~2 μm. We printed the PRTD array designs on chrome photolithography masks, and used these masks in a mask aligner (SUSS MicroTec MA-6) to expose the resist. After development in Microposit CD-30 the slides were plasma-etched briefly (~1 minute) to remove any organic residue from the areas which were exposed and developed.

We loaded the slides in an electron-beam thin-film evaporator (e-beam) and coated them first with titanium and then with platinum. The titanium ensured adhesion of the platinum to the glass, but it also had a negative impact on the reproducibility of the PRTD sensors; we therefore used the thinnest (1-2 nm) Ti layer that still provided adhesion. The Pt layers were deposited at a rate of ~0.2 nm/s and had a thickness of ~150 nm. The Pt-coated slides were unloaded from the e-beam, soaked in acetone for the lift-off of the metal from resist-coated areas, and then cleaned with isopropanol.

Figure S-2.

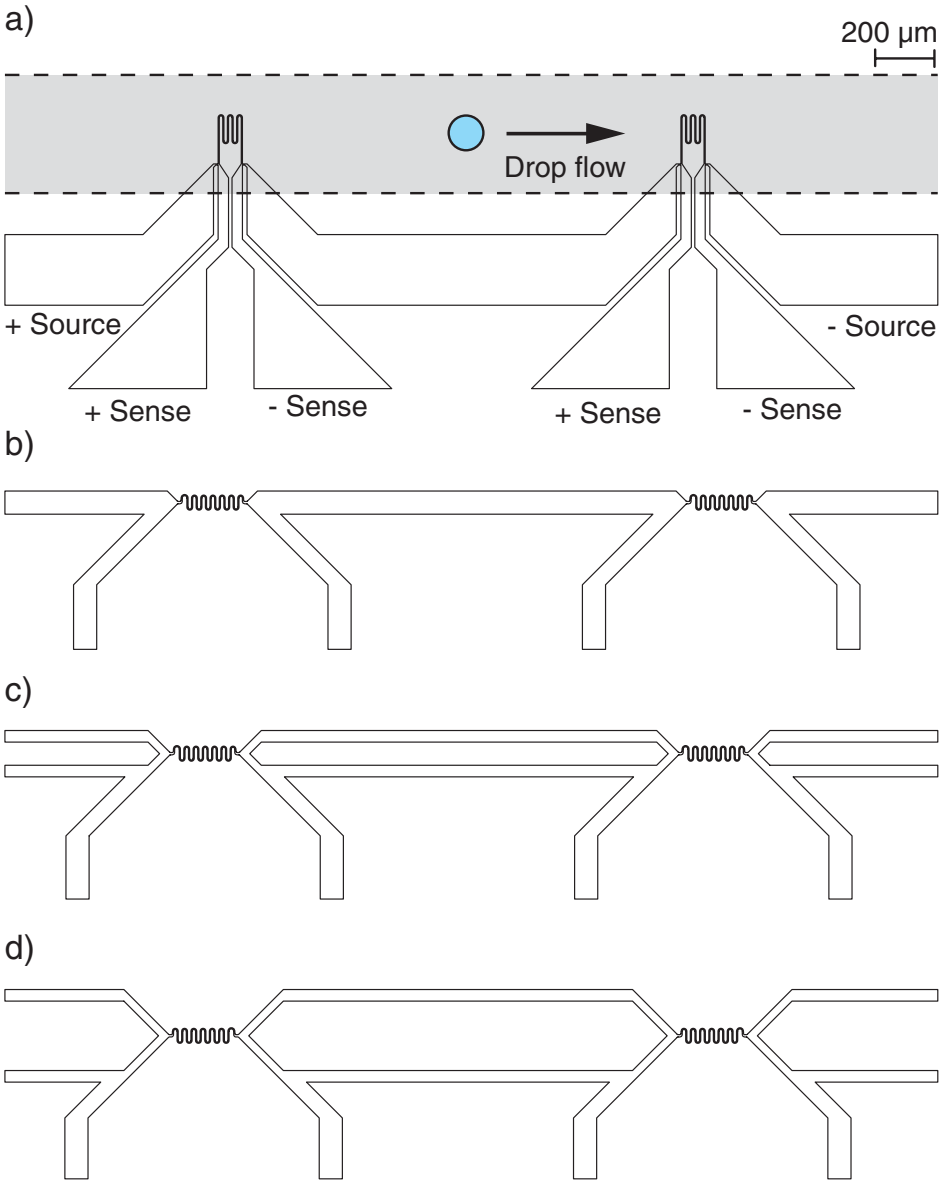

Figure S-2. Drawings, to scale, of the sensors from different PRTD array designs. The scale bar in drawing a) applies to all drawings. Drawing a) also shows the outline of a 400-µm wide channel aligned with the array.

Annealing the PRTD arrays at ~500 ºC for 12 hours lowered the resistance of the sensors and improved significantly their reproducibility. The last fabrication step was to coat the slides (except the leads used for electrical connections) with a 200-nm protective layer of SiO_2 in an e-beam. The SiO_2 layer also provided a surface that could bond to plasma-oxidized PDMS; since PDMS does not bond to platinum layers, bonding a PDMS slab directly to the unprotected arrays could cause leaks of fluid from the device.

The calibration of the PRTD arrays. The calibration procedure was essential for achieving good accuracy in temperature measurements. The main challenge for the accurate calibration of the sensors was the creation of the uniform and stable thermal environment for the sensor arrays. We used a dry calibration scheme using multiple insulation stages to filter out temperature variations and to reduce the drift rate of the temperature.

The complete microfluidic device and a calibrated PRTD thermometer (Hart Scientific 5622-05, calibration accuracy ±0.04 º C) were placed in contact with an aluminum plate (100 mm wide, 150 mm long, and 6 mm thick) using thermal grease. The aluminum plate sat inside an aluminum box with 12-mm thick walls (inner space 115 mm wide, 125 mm long, and 140 mm high). To minimize the thermal conduction between the box and the plate, the plate was placed slanted inside the box and polyurethane foam pads (5 mm thick) were used at the contact points between the plate and the box. A liquid heat exchanger was placed in contact with the thick-walled aluminum box, and the box was placed inside a thermally insulating box with 30-mm thick walls made of expanded polystyrene foam.

To achieve a given calibration temperature, we ran ethanol from a temperature-stabilized bath (Lauda RP 890) through the heat exchanger. Although the temperature of the ethanol in the

bath fluctuated in some cases by as much as 0.1 ºC around the set temperature of the bath, the temperature of the device was practically constant because of the weak thermal coupling between the aluminum box and the plate. The same weak coupling caused a very slow response of the temperature of the device after a change in the set temperature of the bath: the stabilization of temperature of the device took approximately 5 hours.

The sensitivity of the measurement of temperature was good enough to measure drifts smaller than 0.001 ºC/min. In a typical calibration run we measured these drifts, and recorded calibration data only if the temperature drift was equal or less than 0.002 ºC/min. A calibration run consisted of electrical resistance measurements at five or six temperatures between -50 ºC and 50 ºC. For each sensor and calibration temperature we measured the resistance 20 times to reduce the effect of electrical noise.

We fitted the resistance data from the sensors to a parabolic function of temperature; using higher-order polynomial functions of temperature did not improve significantly the quality of the fit. Since the number of calibration temperatures was larger than the number of fit parameters, the fits were over-determined, and we could use the residuals of the fit to evaluate that the precision of the calibration, for a single calibration run, was better than 0.01 ºC. Between different calibrations, the changes in the calibration curves were larger, but these changes are likely to be caused primarily by the handling of the device between calibrations. The calibration coefficients of very thin (~150 nm) PRTDs sometimes changed after the devices were installed on the cold plate. To judge the reproducibility of the calibration, we compared the pairs of calibration that exhibited, over several days, the least drifts. Since in these cases the largest changes were approximately 0.03 ºC, we evaluated that the reproducibility of calibration procedure is equal to or better than 0.03 ºC.

Derivation of the formula for the calculation of ice nucleation rates. The basic formula for the calculation of the freezing rate R_F can be defined by eq. (SE1),

$$R_F = \frac{1}{\delta t}\frac{N_F}{N_L} \tag{SE1}$$

where δt the observation time in seconds, N_F is the number of drops that freeze within δt, and N_L is the number of liquid supercooled drops at the beginning of investigation; the unit of rate is 1/s.

We rewrote eq. (SE1) using the particular conditions of our experiment, in which the temperature decreases during the measurement, and in which we calculate the freezing rate using freezing events from a finite range of freezing temperatures. This range of freezing temperatures corresponds to a range of freezing positions along the channel. Equation (SE1) becomes:

$$R_F = \frac{1}{t(x) - t(x_0)}\frac{N_L(x_0) - N_L(x)}{N_L(x_0)} \tag{SE2}$$

$$R_F = -\frac{T(x_0) - T(x)}{t(x_0) - t(x)}\frac{N_L(x_0) - N_L(x)}{T(x_0) - T(x)}\frac{1}{N_L(x_0)} \tag{SE3}$$

where x_0 is the position in millimeters where the observation starts and x the position in millimeters where it ends. The temperature of the drops at these positions are $T(x_0)$ and $T(x)$, respectively. For the first drop investigated, $t(x_0)$ the time when the drop is at position x_0 and $t(x)$ the time when it is at position x. (Since all the drops are assumed to have identical speeds, the choice of the drop does not influence the calculation of R_F.) $N_L(x_0)$ is the number of liquid drops entering the observation region at x_0, and $N_L(x)$ the number of remaining liquid drops that exit the observation region at x.

Equations (SE2) and (SE3) can be used to calculate the ice nucleation rates if data specific to our experiment (the position-dependencies of the drop speed, drop temperature, and freezing probability) is available. We nevertheless expressed the data using a different set of variables: the individual temperatures at which freezing initiates in a drop, T_F (in ºC), and the rate of change of the temperature at freezing, $(dT/dt)_F$ (in ºC/s). These variables, along with the volume of the sample of water, can be used to compare ice nucleation data produced by different ice nucleation apparatuses because they are not experiment-specific.

To express the freezing rate as a function of temperature, the dependent variable in eq. (SE3) has to be changed from position, *x*, to temperature, *T*. This change of variable is possible if the temperature depends monotonously on the position (i.e. the temperature is always colder at further positions in the channel). For the ice nucleation experiment in pure water that we reported here, this is not the case: the temperature reached a minimum, and then increased before all drops froze. To apply the temperature-dependent formulas that we list here, we discarded from analysis freezing events that occurred while the temperature of the drops increased. We also discarded events occurring at cooling rates between -2 ºC/s and 0 ºC/s because the errors in determining the cooling rate were large in that case.

After the change of variable from *x* to *T*, eq. (SE3) becomes:

$$R_F = -\frac{T_0 - T}{t(T_0) - t(T)} \frac{N_L(T_0) - N_L(T)}{T_0 - T} \frac{1}{N_L(T_0)} \qquad \text{(SE4)}$$

$$R_F(T) = -\left(\frac{dT}{dt}\right)(T) \frac{1}{N_L(T)} \frac{d}{dT}\left(N_L(T)\right) \qquad \text{(SE5)}$$

Here the drops are investigated in a temperature interval spanning from T_0 (the upper temperature) to T (the lower temperature). $N_L(T)$ is the number of drops that froze at temperatures lower than T, and $(dT/dt)(T)$ the rate of cooling (ºC/s) of the drops as a function of

their own temperature; these two functions can be evaluated numerically from the experimental data on freezing temperatures and on cooling rates.

The generalization of the calculation of freezing rates for the case in which the temperature of the channel fluctuates. The derivation of eq. (SE5) assumes that all drops cool in exactly the same fashion (i.e. when drops reach a given position in the channel, they have the same temperature). This is not always the case for out apparatus, because the temperatures along the channel can fluctuate during the recording of a data set.

The generalization of eq. (SE5) must allow the calculation of freezing rates for arbitrary pairs of freezing temperatures and cooling rates. Once the temperatures (and also the cooling rates) start to fluctuate, the set of freezing events is no longer a statistical ensemble of identical systems, and the problem of measuring the freezing rates becomes one of averaging the results of different experiments. To generalize eq. (SE5) we averaged the freezing rate given by eq. (SE1). We used the following averaging formula, (SE6),

$$R_F(T,\Delta T) = \frac{\sum_{d=1}^{Total\ number\ of\ drops} \frac{1}{\delta t_d} f_d}{\sum_{d=1}^{Total\ number\ of\ drops} l_d} \qquad \text{(SE6)}$$

where $R_F(T,\Delta T)$ is the rate of freezing at temperature T calculated across a finite temperature bin of width ΔT (spanning from $T-\Delta T/2$ to $T+\Delta T/2$), d is the drop indexing number, δt_d is the passage time of droplet d through the temperature bin ΔT, and the functions f_d and l_d are defined as follows:

$$f_d = \begin{cases} 1, \textit{ if d freezes between } T+\frac{\Delta T}{2} \textit{ and } T-\frac{\Delta T}{2} \\ 0, \textit{ otherwise} \end{cases} \qquad \text{(SE7)}$$

$$l_d = \begin{cases} 1, \ if \ d \ is \ liquid \ when \ reaching \ T + \dfrac{\Delta T}{2} \\ 0, \ otherwise \end{cases} \tag{SE8}$$

Equation (SE6) can be easily adapted to use experimental data as its input variables:

$$R_F(T, \Delta T) = \frac{1}{\Delta T} \frac{\sum_{d=1}^{Total \ number \ of \ drops} \left(\frac{dT}{dt} \right)_d (T_{freeze}) f_d}{\sum_{d=1}^{Total \ number \ of \ drops} l_d} \tag{SE9}$$

where $(dT/dt)_d(T_{freeze})$ is the rate of cooling of drop d when it freezes at the temperature $T_{freeeze}$. The evaluation of functions f_d and l_d requires only the comparison of the freezing temperature of drop d with the upper and lower bin temperatures.

Equation (SE9) reduces to eq. (SE5) for drops cooling in the same fashion, and is accurate if the ratio of the number of drops frozen inside the bin to the starting number of liquid drops is small (<~0.1). If this ratio is large (>~0.1), eq. (SE9) underestimates the freezing rate when freezing is a stochastic process. For our experimental ice nucleation data, the ratio of frozen to liquid drops was small for most of the temperature bins, because of the large number of freezing events that we recorded. Nevertheless, this ratio became large at the lowest temperatures. For the calculation of homogenous nucleation rates we corrected the nucleation rate according to the formula:

$$J_{corr}(T, \Delta T) = J(T, \Delta T) \frac{-\ln\left(1 - \dfrac{\sum_{d}^{All \ drops} f_d}{\sum_{d}^{All \ drops} l_d}\right)}{\left(\dfrac{\sum_{d}^{All \ drops} f_d}{\sum_{d}^{All \ drops} l_d}\right)} \tag{SE10}$$

where $J_{corr}(T,\Delta T)$ and $J(T,\Delta T)$ are the corrected, and the uncorrected rates of nucleation calculated at temperature T in a bin of width T. This correction factor is approximate, and we evaluated that it has the effect of overestimating the nucleation rates if the ratio of frozen drops to liquid drops is larger than approximately 0.5.

Other electronic files included in the supplementary information. The other files included with the supplementary information are the freezing temperature and cooling rate data for ice nucleation experiments on pure water, and seeded with silver iodide; and six movies of freezing drops inside microfluidic channels.

Raw data from ice nucleation experiments. These two text files are named *'Stan_Whitesides_2008-Jun-04_Freezing_Temperatures_37211_Pure_Water_Drops.rtf'*, and *'Stan_Whitesides_2008-Dec-23_Freezing_Temperatures_8900_AgI-seeded_Water_Drops.rtf'*. They contain the freezing temperatures, and cooling rates at the moment of freezing, for all the data we reported in this paper. The data is listed in a tab-delimited format, and the file contains a text header containing the descriptions of the experiment and of the data listed in the file. The data can be imported into most spreadsheet computer programs if the text header is deleted.

Movies of freezing drops in a microfluidic channel. The first four out of six movies are uncompressed. Except for image cropping and for selection of a frame range for the purpose of reducing the size of the files, these four movies were not processed after they have been downloaded from the camera. The file names list the recording frame rate of the movie, and the size of the imaged area.

The last two movies are video presentations of the freezing processes. They use the uncropped raw footage from the first two movies, and were edited by adding dynamic text descriptions.

i) *'Stan_Whitesides_2007-Aug-02_CompleteImageFreezing_AgI-seeded_Water_1000fps_15000x563micron.avi':*

This movie shows the full sequence of drop handling: generation, cooling, and freezing. A full frame from this movie is sown in figure 6a.

ii) *'Stan_Whitesides_2006-Dec-21_HighResolutionFreezing_Pure_Water_16000fps_1791x223micron.avi':*

This movie shows with high temporal and spatial resolution the two-step process of freezing in supercooled water: first the rapid formation of ice dendrites, and then the more gradual freezing of the rest of the water inside the drop. The sequence of images in figure 6b was extracted from this movie.

iii) '*Stan_Whitesides_2008-Jun-04_FreezingMovieSection_Pure_Water_1000fps_11682x308micron.avi':*

This movie is part of the actual movie recorded for the measurement of homogenous nucleation rates; the image in this movie was not cropped.

iv) *'Stan_Whitesides_2008-Dec-23_FreezingMovieSection_AgI-seeded_Water_1400fps_5462x202micron.avi'*:

This movie is part of the actual movie recorded for the measurement of heterogeneous nucleation rates; the image in this movie was not cropped.

v) *'Stan_MicrofluidicIceNucleation_YouTube-Part1_090506.mov'*

Movie presentation based on the movie (i) showing the full sequence of drop handling. The footage used in this presentation shows only homogenous freezing events.

vi) *'Stan_MicrofluidicIceNucleation_YouTube-Part2_090506.mov'*

Movie presentation based on the movie (ii) showing the freezing process imaged with high spatial and temporal resolution.